Journal of Sound and Vibration (1998) **209**(1), 61–76

A THREE-DIMENSIONAL FLUID–STRUCTURE COUPLED ANALYSIS OF ROTATING FLEXIBLE ASSEMBLIES OF TURBOMACHINES

G. Jacquet-Richardet and P. Rieutord

Laboratoire de Mécanique des Structures—UPRESA CNRS 5006, *INSA de Lyon*, 20 *Avenue Albert Einstein*, 69621 *Villeurbanne Cedex*, *France*

(*Received* 29 *November* 1996, *and in final form* 22 *July* 1997)

Numerous experimental and numerical studies have shown that the stability of rotors is strongly influenced by fluid elements. When considering elements such as journal bearings or seals, the classical rotordynamic approach has been widely used and validated. On the other hand, the rigid wheel assumption seems questionable when considering elements such as fluid leakage at blade tip or secondary flow passages of shrouded impellers. In this paper, a coupling technique between a fluid and a fully three-dimensional rotating flexible wheel shaft assembly is presented. This coupling technique considers alternatively the governing equations of fluid and structure and is based on an interfacing grid concept associated with a modal representation of the coupled system. A first simple application is used for illustrating and validating the proposed method. Computed results are compared to results given by a classical rotordynamic approach. Then the method is applied to a test flexible wheel–shaft–bearing assembly. Various configurations are studied and the influence of wheel flexibility on the overall behaviour is illustrated in all cases.

1. INTRODUCTION

Most of the self-excited motions within turbomachines are caused by fluid forces acting on the rotor, when energy is transmitted from rotation to vibration [1–4]. Lomakin [5] first showed the major influence that seals have on the rotordynamic response of centrifugal pumps. More recently, numerous experimental and numerical studies [6] have shown that the stability of rotors is strongly affected by fluid elements such as journal bearings, seals, fluid leakage at blade tip or secondary flow passages of shrouded impellers. The high pressure, high speed and small clearances needed to raise efficiency and prevent leakage induce large fluid forces which can cause instability.

The global analysis of the dynamic behaviour of rotating wheel–shaft assemblies is mostly performed by using the rotordynamic approach [7]. The shaft is modelled as a beam, the wheels are assumed to be rigid and the fluid forces are reduced to their integrated effect on the shaft centre line. For the structure, the finite element method is often used. The shaft is discretized by using beam elements and the wheels are accounted for by their global mass and inertia. Reliable modelling of the dynamic characteristics of fluid elements started fairly recently. The bulk flow model, developed by Childs [8, 9], is a predictive tool widely used to compute the direct and cross-coupled rotordynamic coefficients for annular seals. With this model, the governing equations are linearized by using a perturbation analysis for small motions about a centred position. The force coefficients are found by integration of the first order pressure perturbations along and around the shaft. The classical bulk flow model was extended by Childs [10] for computation of the rotordynamic

0022–460X/98/010061 + 16 $25.00/0/sv971225

coefficients induced by shrouded impeller surfaces. Ditzen and Nordmann [11] developed a finite difference technique to compute seal coefficients. Despite the complex nature of these analyses, they involve geometry-related restrictions and their accuracy naturally declines in the case of generally shaped annular flow passages. For modelling geometries ranging from the housing of an annular seal on the simple end to the shroud-seal assembly of an impeller stage on the complex end, Baskharone and Hensel [12] proposed a perturbation technique based on a finite element discretization.

In only a small number of studies has the possible interaction between fluid and local structural deformations been considered. Iwatsubo and Yang [13] analyzed the effect on seal dynamics of elastic changes of shaft and seal diameters induced by high pressures. They showed that the direct stiffness coefficient is significantly influenced by these deformations and that the damped critical speed of first and second modes is increased. Desbordes *et al*. [14] analyzed the influence of elastic deformation of pads on shaft trajectory inside a three shoe tilting pad bearing. They showed that pad distortion may largely increase the orbit amplitude and maximum pressure. Frêne *et al*.[15] showed that geometry defects related to deformation or to manufacturing tolerances may have important effects.

On examining the published studies, it appears that journal bearings and seals have already received considerable attention. Within this field of application, the classical rotordynamic approach has been largely validated and seems accurate enough. On the other hand, it appears that interactions involving wheels have not been analyzed sufficiently. Initially, impellers were thought to create relatively benign rotordynamic destabilizing forces [16]. More recently, Childs [10] showed that forces developed within the leakage path between impeller shroud and pump housing are significant, and can even dominate the resultant forces for reduced clearances. The effect of these forces appears to be strongly dependent on geometrical configurations and working conditions.

Concerning this latter field of research, two main questions remain open: (i) what are the validity limits of the rigid wheel assumption applied to shrouded impeller fluid structure interactions?; (ii) which basic models and coupling techniques should be used when the accuracy of the rotordynamic approach seems questionable?

The aim of the work presented is to propose a solution to the second question, in order to obtain a better understanding concerning the first.

2. FLUID–STRUCTURE MODELLING: COUPLING TECHNIQUE

Good prediction of the coupled behaviour of flexible wheel–shaft assemblies requires three elements of equal importance: first, accurate basic structural and fluid models, adapted to complex geometry and including all the important effects; and, second, an appropriate coherent coupling technique between these two models. The structural model considered has already been presented and validated in previous papers [17, 18] and thus will be described only briefly here. The development of a fluid model is beyond the scope of this study, especially since efficient and well adapted approaches already exist. Thus, the participation of the fluid is considered as generally as possible. The coupling technique, developed with both efficiency and flexibility requirements to link fully three-dimensional structural and fluid models, is presented. For application and validation, the problem is particularized to the classical rotor–bearing interaction.

2.1. GOVERNING EQUATIONS

The basic structural model considered is based on three-dimensional finite element discretization. Rotational effects such as centrifugal and gyroscopic effects are accounted

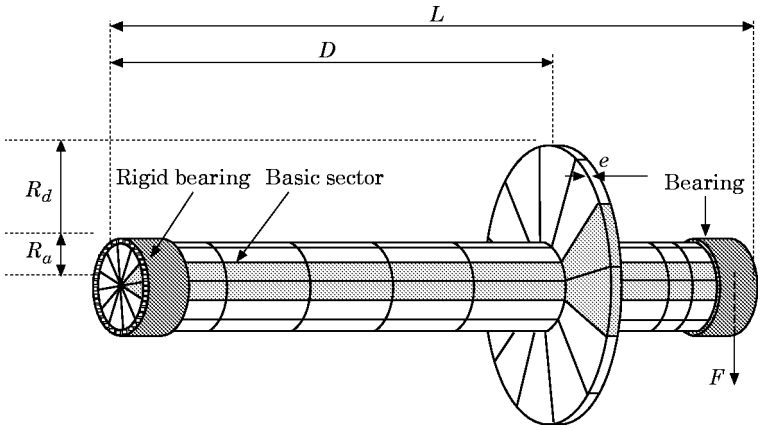

Figure 1. A simple axisymmetrical disc–shaft assembly. Dark elements: basic cyclic symmetrical sector.

for and couplings between the flexible wheel and the flexible shaft are possible. In view of the large number of degrees of freedom needed for accurate analyses, full advantage is taken of the cyclic symmetrical property of the structure. Thus, the governing equations associated with the dynamic problem are written as

$$[M(\beta_n)]\{\ddot{\delta}_n\} + [C(\beta_n)]\{\dot{\delta}_n\} + [K(\beta_n)]\{\delta_n\} = \{F_n\}, \tag{1}$$

where $[M]$ is the mass matrix, $[C]$ is the gyroscopic matrix, $[K]$ is the stiffness matrix including centrifugal stress stiffening and spin softening, $\{\delta_n\}$ is the nodal displacement vector and $\{F_n\}$ is the vector of nodal forces applied to the structure. The different quantities in equation (1) are associated with a reference cyclic sector. The behaviour of the whole system is accounted for by parameter β_n, which gives a phase relation between

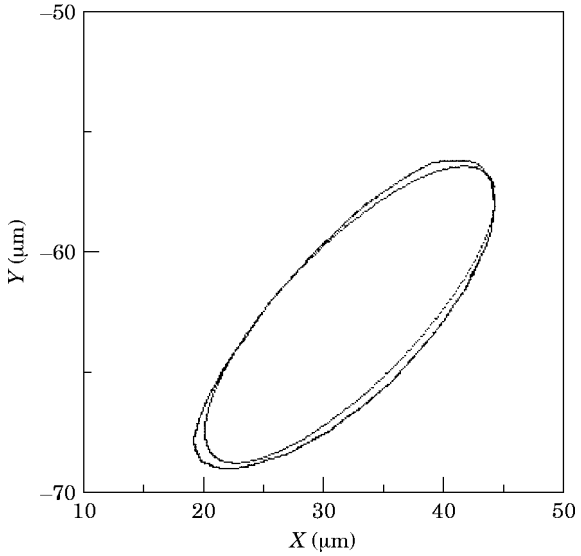

Figure 2. A stabilized orbit at bearing level: a comparison between computed results and results given by a classical rotordynamic approach.

the displacements and the forces of the different sectors p and a reference sector, as in the following:

$$\{\delta^{(p)}\} = \{\delta_n^c\} \cos (p-1)\beta_n + \{\delta_n^s\} \sin (p-1)\beta_n, \tag{2}$$

$$\{F^{(p)}\} = \{F_n^c\} \cos (p-1)\beta_n + \{F_n^s\} \sin (p-1)\beta_n. \tag{3}$$

As symbolized in equation (1) by subscript n, the reduced dynamic problem has to be solved for each of the possible discrete values of β_n, given by

$$\beta_n = 2\pi n/N, \qquad n \in [0, N^*/2], \tag{4}$$

where N is the total number of cyclic sectors and $N^* = N$ if N is even or $N^* = N - 1$ if N is odd. The cyclic symmetrical forces vectors $\{F_n\}$ are obtained from the full forces vector applied to the entire structure, as shown in the Appendix.

Solving equation (1) directly remains too cumbersome for realistic models. As proposed and validated in references [17, 18], the non-rotating problem is solved first, giving a set of mode shapes $[\psi_n]$ that are used to reduce the rotating probelm (1). Upon assuming that

$$\{\delta_n\} = [\psi_n]\{q_n\}, \tag{5}$$

system (1) becomes

$$[m_n]\{\ddot{q}_n\} + [c_n]\{\dot{q}_n\} + [k_n]\{q_n\} = \{f_n\}, \tag{6}$$

where $[m_n]$, $[c_n]$ and $[k_n]$ are, respectively, the modal mass, gyroscopic and stiffness matrices. The modal forces vector, $\{f_n\}$ is obtained from

$$\{f_n\} = [\psi_n]\{F_n\}. \tag{7}$$

2.2. COUPLING TECHNIQUE

Techniques used classically within the rotordynamic approach, to couple structural and fluid models, remain simple for two main reasons. First, the rotating structure is considered to be axisymmetric, allowing modelling with respect to the fixed inertial reference frame without the emergence of periodic coefficients. Second, the interaction between the fluid and the rotating structure is considered in a global integrated way, leading to coefficients that are directly compatible with beam modelling.

In regard to the interaction between a fluid and a fully three-dimensional rotating flexible wheel–shaft assembly, the coupling techniques involved are inevitably more complex. Several methods exist, mainly developed within the field of aeroelasticity. Strong coupling methods, which involve solving the coupled problem with the same type of discretization and numerical schemes for fluid and structural domains, were not considered. When using these methods the coupling is simplified but the computational effort needed is much too great. Furthermore, a coupling technique should be flexible, as designers like to be able to use different elements for each domain and to refine and validate each mesh independently. More flexible methods consider the governing equations of fluid and structure alternatively, with data being passed as a boundary condition between the two domains [19]. By applying these methods to the problem considered, the following difficulties have to be solved. (i) *Frame difference*: the cyclic symmetrical structure shall be described with respect to the rotating frame, while the fluid is usually described with respect to the fixed inertial frame. (ii) *Discretization difference*: the structure is modelled by using finite elements with displacement degrees of freedom, while the fluid is modelled by using both finite elements and finite differences with pressure degrees of freedom; the mesh needed for the fluid is usually far more dense than the mesh needed for the structure.

(iii) *Information loss*: the transfer of fluid data is critical, since it concerns highly non-linear data, with important variation gradients both in space and time; furthermore, this transfer is done from the fine mesh to the coarser mesh. (iv) *Relative motions*: due to rotation, the relative position of fluid and structural meshes is not stationary at the interface between the two coupled domains.

The first and last points are dealt with by using a time marching integration procedure. The problem of discretization difference and information loss are dealt with by using an

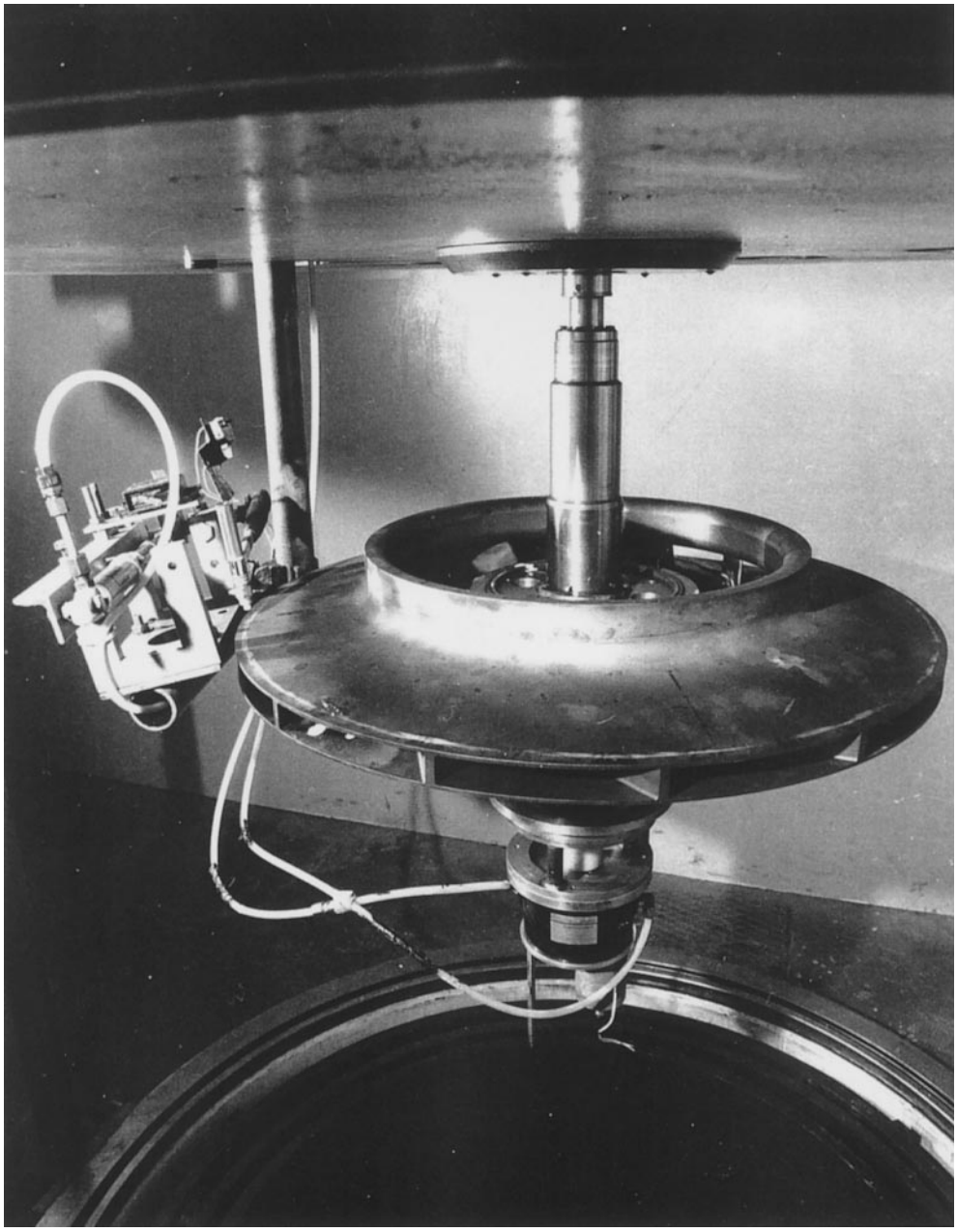

Figure 3. The test compressor wheel–shaft assembly (courtesy of Framatome Thermodyn).

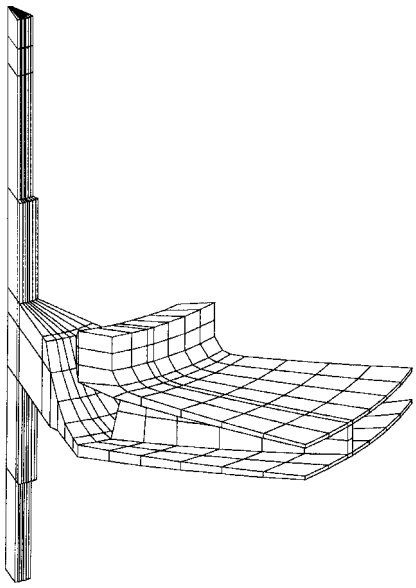

Figure 4. The finite element mesh of the basic sector (1/13th of the entire assembly).

interfacing grid associated with a modal representation of the coupled system [20, 21]. The modal quantities are physical and thus are independent of the frame or of the mesh, provided that the latter is fine enough to satisfy accuracy requirements. As described in reference [17], the structural modal quantities, involved in equation (6), are computed by using the structural mesh. Instead of calculating fluid modal quantities after projection on to the structural mesh, they are directly computed by using an interfacing grid concept. The interfacing grid [21] is constituted of planar four-noded finite elements, moves with

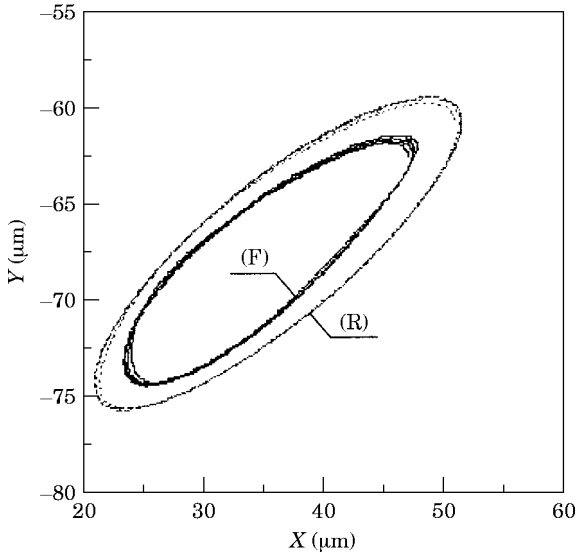

Figure 5. The stabilized orbit at bearing level; $\Omega = 6000$ rpm, $\mu = 0{\cdot}01$ Pa.s. (F), Flexible wheel (proposed approach); (R), rigid wheel (rotordynamic approach).

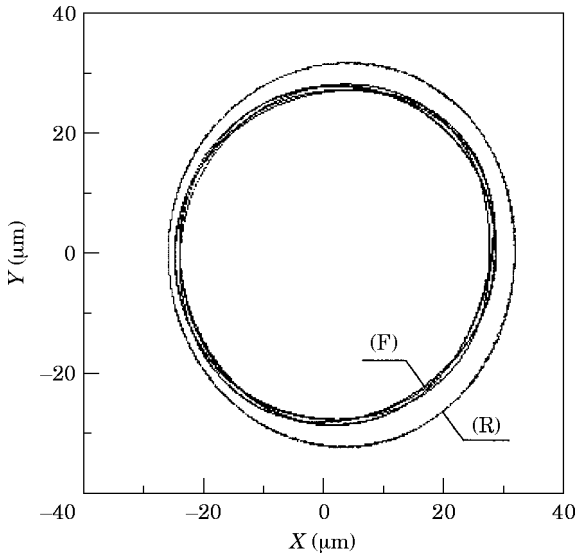

Figure 6. The stabilized orbit at wheel level; $\Omega = 6000$ rpm, $\mu = 0{\cdot}01$ Pa.s. (F), Flexible wheel (proposed approach); (R), rigid wheel (rotordynamic approach).

the structure and is initially identical to the fluid mesh at the fluid–structure boundary. For coupling, two transfers are needed. The first is for structural displacements from the structural mesh to the interfacing grid. This transfer is simple because it involves data with smooth variations (mode shapes), and is done from the coarse mesh to the fine mesh. The second concerns fluid pressures, and is done from the fluid mesh to the interfacing grid. Considering the nature of the interfacing grid, this last transfer is straightforward.

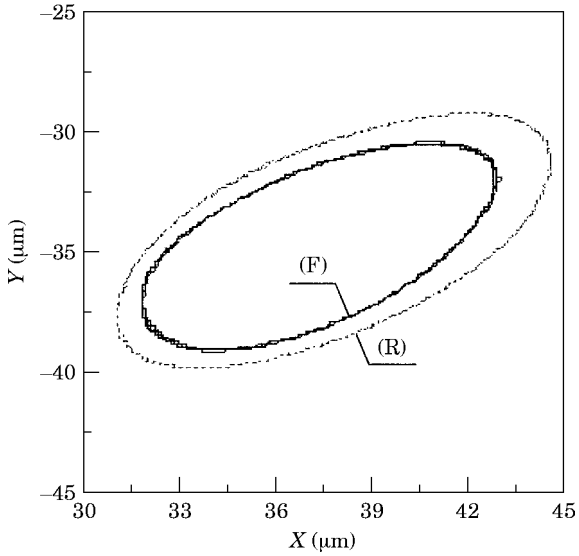

Figure 7. The stabilized orbit at bearing level; $\Omega = 6000$ rpm, $\mu = 0{\cdot}05$ Pa.s. (F), flexible wheel (proposed approach); (R), rigid wheel (rotordynamic approach).

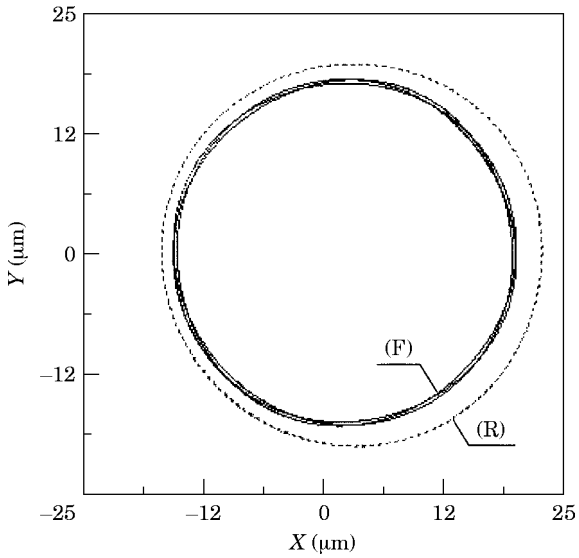

Figure 8. The stabilized orbit at wheel level; $\Omega = 6000$ rpm, $\mu = 0{\cdot}05$ Pa.s. (F), Flexible wheel (proposed approach); (R), rigid wheel (rotordynamic approach).

The coupling process involves the following steps:

1. Computation of mode shapes $[\psi_n^s]$ associated with the uncoupled structure at rest, using the structural mesh. Computation of the structural modal matrices.
2. Mode shape transfer from the structural mesh $[\psi_n^s]$ to the interface grid $[\psi_n^I]$.
3. Initialization of the solution $\{q_n\} = 0$.

Then, beginning of the iterative process:

4. Computation of forces applied to the structure $\{F^e\}$ (unbalance, excitation, etc), excluding forces associated with the fluid–structure interaction. Computation of the

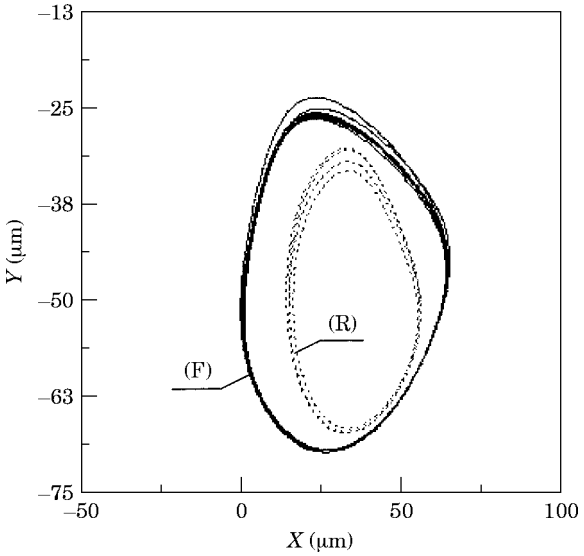

Figure 9. The stabilized orbit at bearing level; $\Omega = 11\,800$ rpm, $\mu = 0{\cdot}01$ Pa.s. (F), Flexible wheel (proposed approach); (R), rigid wheel (rotordynamic approach).

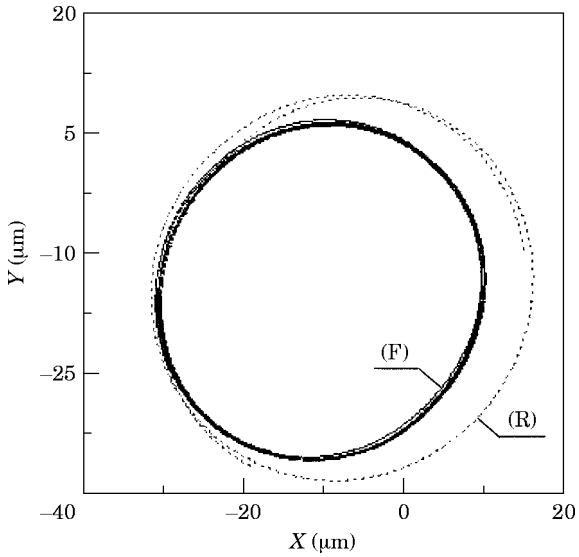

Figure 10. The stabilized orbit at wheel level; $\Omega = 11\,800$ rpm, $\mu = 0{\cdot}01$ Pa.s. (F), Flexible wheel (proposed approach); (R), rigid wheel (rotordynamic approach).

associated modal forces $\{f_n^e\}$, according to equation (7), after cyclic symmetrical decomposition via equations (A2, A3) of the Appendix.

5. Solution of system (6) giving $\{q_n\}$. Computation of the cyclic symmetrical generalized displacements at the interface, $\{\delta_n^I\} = [\psi_n^I]\{q_n\}$. Computation of the physical displacements with respect to the rotating frame according to equation (A4), giving $\{\delta^I\}$.

6. Transformation of these displacements from the rotating frame $\{\delta^I\}$ to the fixed inertial frame $\{\overline{\delta}^I\}$. Generation of a new fluid mesh.

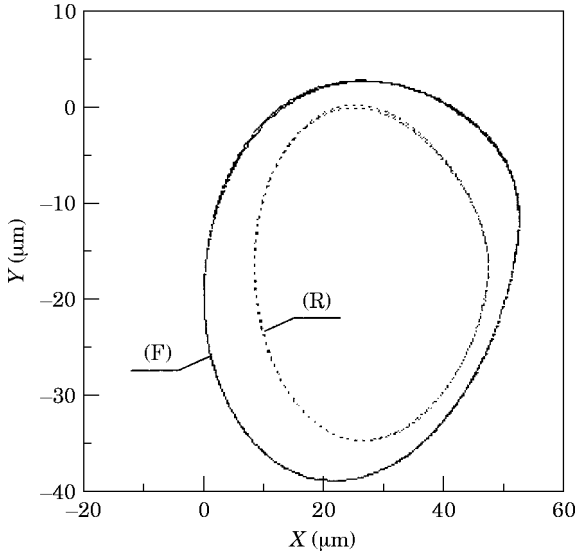

Figure 11. The stabilized orbit at bearing level; $\Omega = 11\,800$ rpm, $\mu = 0{\cdot}05$ Pa.s. (F), Flexible wheel (proposed approach); (R), rigid wheel (rotordynamic approach).

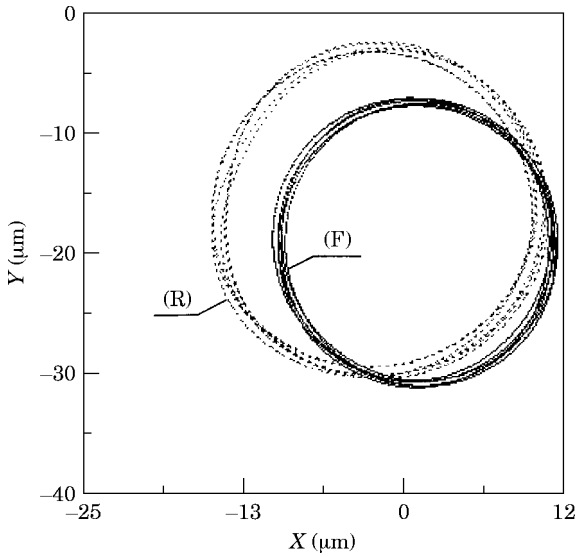

Figure 12. The stabilized orbit at wheel level; $\Omega = 11\,800$ rpm, $\mu = 0{\cdot}05$ Pa.s. (F), Flexible wheel (proposed approach); (R), rigid wheel (rotordynamic approach).

7. Computation of the fluid pressures generated at the interfaces. Computation of the associated modal equivalent forces $\{\bar{F}^I\}$. Transformation of $\{\bar{F}^I\}$ into the rotating frame, giving $\{F^I\}$.

8. Decomposition of $\{F^I\}$ into cyclic symmetrical generalized forces $\{F_n^I\}$. Computation of the associated modal forces $\{f_n^h\} = [\psi_n^I]\{F_n^I\}$.

Steps 4–8 are repeated until the solution converges.

The integration scheme used is the fourth order Runge–Kutta method, which appears to be efficient in the case of non-linear systems [22]. For modal quantities, the cyclic

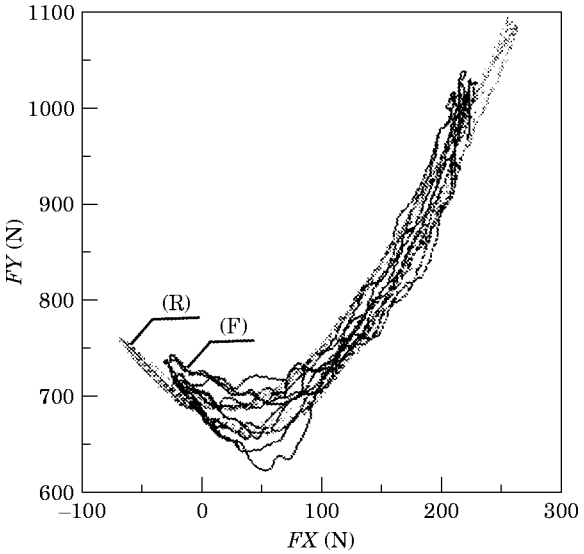

Figure 13. The resultant of the hydrodynamic forces in the bearing; $\Omega = 6000$ rpm, $\mu = 0{\cdot}01$ Pa.s. (F), Flexible wheel (proposed approach); (R), rigid wheel (rotordynamic approach).

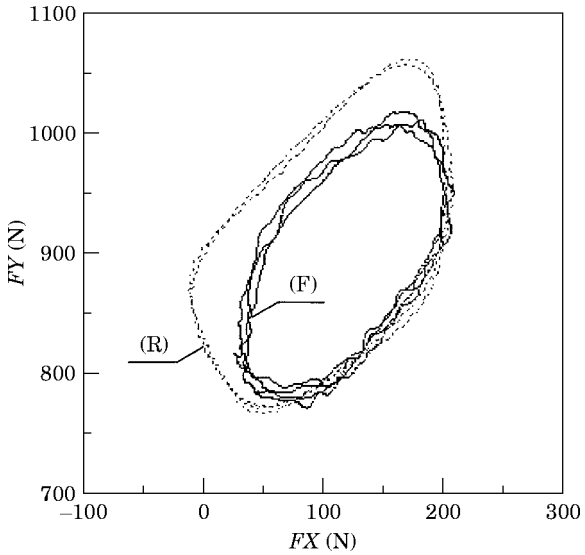

Figure 14. The resultant of the hydrodynamic forces in the bearing; $\Omega = 6000$ rpm, $\mu = 0{\cdot}05$ Pa.s. (F), Flexible wheel (proposed approach); (R), rigid wheel (rotordynamic approach).

symmetrical decomposition is not essential for the coupled analysis. The decomposition is retained to lower the computational memory resources needed and to facilitate the interpretation of the results.

3. APPLICATION

For the application, the method is particularized to the classical case of rotor–journal bearing interaction. As the main interest of the proposed method lies in the interaction

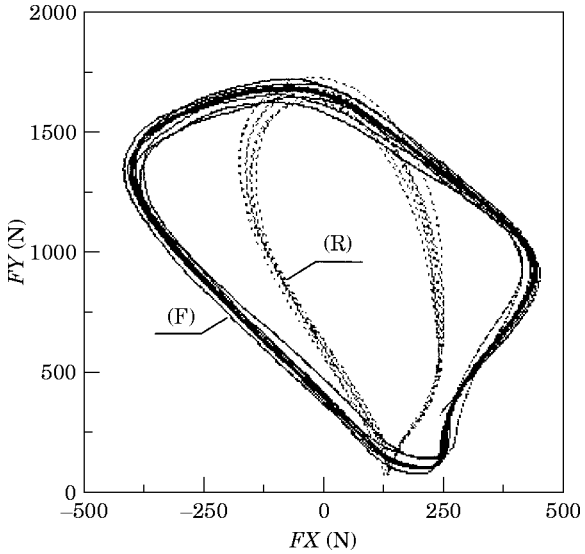

Figure 15. The resultant of the hydrodynamic forces in the bearing; $\Omega = 11\,800$ rpm, $\mu = 0{\cdot}01$ Pa.s. (F), Flexible wheel (proposed approach); (R), rigid wheel (rotordynamic approach).

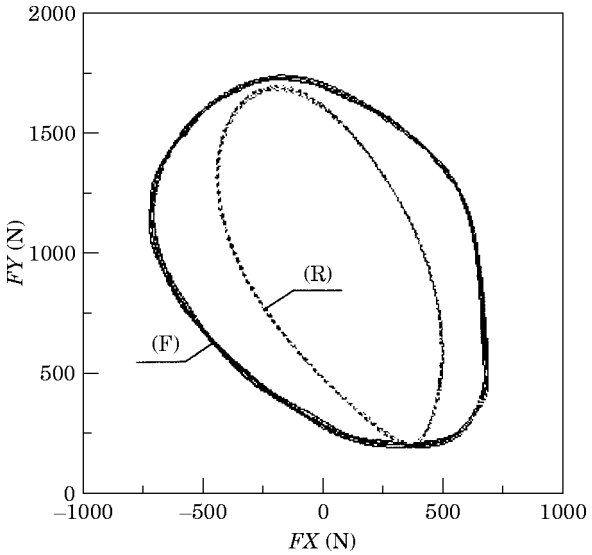

Figure 16. The resultant of the hydrodynamic forces in the bearing; $\Omega = 11\,800$ rpm, $\mu = 0{\cdot}05$ Pa.s. (F), Flexible wheel (proposed approach); (R), rigid wheel (rotordynamic approach).

involving shrouded assemblies, this application is not thought to bring additional physical understanding to the problem. However, before considering more challenging problems, it has been judged essential to consider a well known case, in order to illustrate and validate the process developed. The method is first validated by using a simple application. Then a test wheel–shaft assembly is considered and the influence of wheel flexibility on the overall behaviour is highlighted.

3.1. BASIC HYDRODYNAMIC EQUATION

The flow in the bearing is assumed to be laminar and without inertia. For an incompressible fluid, without an effect of temperature, the pressure in the film is governed by the classical Reynolds equation [2, 15]

$$\frac{1}{R}\frac{\partial}{\partial\theta}\left[h^3\frac{\partial P}{\partial\theta}\right]+\frac{\partial}{\partial z}\left[h^3\frac{\partial P}{\partial z}\right]=6\mu\Omega\frac{\partial h}{\partial\theta}+12\mu\frac{\partial h}{\partial t}, \tag{8}$$

where μ is the dynamic viscosity of the fluid, Ω is the rotational angular speed of the rotor, h is the film thickness and P is the pressure in the film. Equation (8) is solved by using the finite difference method, associated with a Gauss/Seidel iterative procedure with over-relaxation. Reynolds boundary conditions are considered.

3.2. SIMPLE APPLICATION

The system presented in Figure 1, is composed of an axisymmetrical disc–shaft assembly, rigidly supported at one end and mounted on a short bearing at the other end. The length of the bearing is $l = 0{\cdot}02$ m, its radial clearance is $C = 10^{-4}$ m and the viscosity of the fluid is $\mu = 0{\cdot}01$ Pas. The length of the shaft is $L = 0{\cdot}65$ m and its radius is $R_a = 0{\cdot}04$ m. The radius of the disc is $R_d = 0{\cdot}2$ m and its thickness is $e = 0{\cdot}02$ m. The disc is mounted at $D = 0{\cdot}5$ m from the rigid bearing. A vertical force $F = 1000$ N is applied to the rotor at the bearing level.

TABLE 1

Equilibrium position and associated hydrodynamic forces

	Reference results, rotordynamic approach	Computed results, proposed approach	Δ (%)
X (m)	$0{\cdot}327 \times 10^{-4}$	$0{\cdot}316 \times 10^{-4}$	3·3
Y (m)	$-0{\cdot}602 \times 10^{-4}$	$-0{\cdot}633 \times 10^{-4}$	5·1
FX (N)	140	150	7·1
FY (N)	747	694	7·9

With the approach considered, 1/6th of the entire axisymmetrical assembly is modelled by using 30 isoparametric brick finite elements with 20 nodes. The same assembly is also modelled with a rotordynamic approach [7, 23] by using 15 beam finite elements for the shaft discretization. For compatibility requirements, the disc is supposed to be rigid in both cases. Frequency computation and response to unbalance, performed on the isolated structure [24], show a 5% difference between the results given by the two models. For the coupled system, two series of data are compared: first, the equilibrium position in the housing of the rotor rotating at 10 000 rpm and the associated hydrodynamic resultant forces (see Table 1); and, second, the stabilized orbit, at bearing level, of the rotor submitted to an unbalance of 10 gm/cm located on the disc (see Figure 2).

On examining Table 1 and Figure 2, it appears that the results computed totally independently by using the proposed method and a classical rotordynamic approach are in good agreement. The discrepancies noticed for the coupled system are of the same order of magnitude as those noticed for the isolated structure.

3.3. APPLICATION TO A WHEEL–SHAFT–BEARING ASSEMBLY

The method is applied to the test compressor wheel–shaft assembly, developed and tested by Framatome Thermodyn [25], and already considered in reference [17]. The main dimensions of the structure, presented in Figure 3, are as follows: (1) impeller outer diameter = 0·685 m, impeller inner diameter = 0·196 m, height = 0·120 m, mass = 60·3 kg; (2) shaft length = 0·5 m, shaft diameter at both ends = 0·06 m. As shown in Figure 4, only 1/13th of the entire assembly is meshed by using 269 brick finite elements with 20 nodes (5925 degrees of freedom). The structural modelling was validated previously by using both experimental and numerical results. Computations, presented in reference [17], have shown the significant influence of wheel flexibility on the overall dynamic behaviour of the simply supported assembly.

As with the previous application, the rotor is assumed here to be rigidly supported at one end and mounted in a journal bearing at the other end. The length of the bearing is $l = 0{\cdot}024$ m, the radial clearance is $C = 10^{-4}$ m and two different fluid viscosities are considered: $\mu_1 = 0{\cdot}01$ Pas and $\mu_2 = 0{\cdot}05$ Pas. The fluid mesh is a finite difference mesh constituted with 182 nodes in the circumferential direction and 12 nodes in the axial direction. Compared to the structural mesh, the fluid mesh is six times finer in the circumferential direction and twice as fine in the axial direction. A vertical force $F = 1000$ N is applied to the rotor at the bearing level and an unbalance of 50 gm/cm is located on the wheel. After a few trials, the time step was set at $\Delta t = 10^{-6}$ s. In view of the very considerable computational effort needed, only two rotation speeds were considered. The first is $\Omega_1 = 6000$ rpm and the second, $\Omega_2 = 11\,800$ rpm, is close to the first critical speed of the rotor. The initial rotor position is assumed to be at the bearing centre. Computations were performed until a stabilized orbit was obtained. Two orbits are

presented, the first at the bearing level and the second at the wheel level. In all cases, the influence of wheel flexibility is highlighted.

As shown in reference [17], the results given by the flexible wheel model are very close to those given by the rotordynamic model when the wheel stiffness is increased. Consequently, the influence of wheel flexibility is fully illustrated by the differences between the rotordynamic results, referenced R (rigid wheel), and the results given by the proposed model, referenced F (flexible wheel). The orbits computed at 6000 rpm are presented in Figures 5–8. At 6000 rpm, wheel flexibility induces a global decrease in the amplitude of the orbit. The orbit at bearing level remains elliptic and the orbit at wheel level remains globally centred. As shown in Figures 9–12, the influence of wheel flexibility is more complex at 11 800 rpm. When considering wheel flexibility, the orbit at bearing level is no longer elliptic and becomes larger than the rigid wheel orbit. These tendencies are confirmed by the shapes of the resultant of the hydrodynamic forces, presented in Figures 13–16.

4. CONCLUSIONS

For an accurate prediction of the dynamic behaviour of rotors, one should consider the coupling mechanisms between the vibrating structure and the surrounding fluid, as well as the coupling mechanism between the different flexible parts of the assembly. When the effect of wheel flexibility can be neglected, the classical rotordynamic approach is a powerful tool. In this work the case in which wheel flexibility effects are significant has been considered and an adapted coupling technique has been proposed. The coupling technique involves use of an interfacing grid between the two domains and is based on a modal representation of the coupled system. A first application, on a simple axisymmetrical disc shaft assembly, shows that the proposed technique does not reduce the quality of the model. The validation is based on the comparison between results computed by using the proposed approach and results computed independently by using a rotordynamic approach. Then a test compressor wheel–shaft assembly, mounted on a rigid bearing at one end and on a journal bearing at the other end, has been considered. The results computed show the significant effect of wheel flexibility on shaft bending modes. This influence reduces or increases the rotor orbits, depending upon the configuration considered.

ACKNOWLEDGMENTS

The authors wish to express their thanks to Dr. O. Bonneau, Université de Poitiers, for providing the reference results used for the first application, and to Framatome Thermodyn for providing the geometry of the wheel–shaft assembly considered for the second application. They would also like to thank Alsthom-Bergeron, Electricité de France, Framatome Thermodyn and the Ministère de l'Enseignement et de la Recherche, for the financial support.

REFERENCES

1. W. Diewald and R. Nordmann 1989 *Transactions of the American Society of Mechanical Engineers*, *Journal of Vibration and Acoustics* **111**, 370–378. Dynamic analysis of centrifugal pump rotors with fluid mechanical interaction.
2. D. W. Childs 1993 *Turbomachinery rotordynamics*: *Phenomena Modeling and analysis*. New York: John Wiley.

3. T. Iwatsubo and B. C. Sheng 1991 *ASME Vibration Conference DE* **37**, 239–244. Stability analysis of turbomachinery from the viewpoint of seals.
4. J. H. Wang and F. M. Shih 1990 *Transactions of the American Society of Mechanical Engineers, Journal of Engineering for Gas Turbines and Power* **112**, 439–444. Threshold performance optimization of a rotor bearing system subjected to leakage excitation.
5. A. Lomakin 1958 *Energomashinostroenie* **4**, 1158. Calculation of critical speed and securing of the dynamic stability of the rotor hydraulic high pressure machines with reference to forces arising in seal gaps.
6. J. J. Verhoeven 1991 *The Shock and Vibration Digest* **23**, 3–17. Rotordynamics of centrifugal pumps: a matter of fluid forces.
7. M. Lalanne and G. Ferraris 1990 *Rotordynamics Prediction in Engineering*. Chichester: John Wiley.
8. D. W. Childs 1983 *Transactions of the American Society of Mechanical Engineers, Journal of Lubrification Technology* **105**, 437–445. Finite length solutions for rotordynamic coefficients of turbulent annular seals.
9. D. W. Childs and C. H. Kim 1985 *Transactions of the American Society of Mechanical Engineers, Journal of Tribology Technology* **107**, 296–306. Analysis and testing for rotordynamic coefficients of turbulent seal with different directionally homogeneous surface roughness treatment for rotor and stator elements.
10. D. W. Childs 1989 *Transactions of the American Society of Mechanical Engineers, Journal of Vibration and Acoustics* **111**, 216–225. Fluid structure interaction forces at pump–impeller–shroud surfaces for rotordynamic calculation.
11. F. J. Ditzen and R. Nordmann 1987 *Transactions of the American Society of Mechanical Engineers, Journal of Tribology* **109**, 388–394. Calculating rotordynamic coefficients of seals by finite difference technique.
12. E. A. Baskharone and S. J. Hensel 1991 *Transactions of the American Society of Mechanical Engineers, Journal of Fluid Engineering* **113**, 353–367. A finite element perturbation approach to fluid/rotor interaction in turbomachinery elements.
13. T. Iwatsubo and B. S. Yang 1988 *Transactions of the American Society of Mechanical Engineers, Journal of Vibration and Acoustics* **110**, 59–64. The effect of elastic deformation on seal dynamic.
14. H. Desbordes, M. Fillon, C. Chan Hew Wai and J. Frene 1995 *Transactions of the American Society of Mechanical Engineers, Journal of Tribology* **116**, 621–628. Dynamic analysis of tilting pad journal bearing. Influence of pad deformation.
15. J. Frene, D. Nicolas, B. Degueurce, D. Berthe and M. Godet 1990 *Lubrification Hydrodynamique*: *Collection de la DER d'Electricité de France, no*. 72. Paris: Eyrolles.
16. V. Bolleter, A. Wyss, I. Welte and R. Sturchler 1987 *Transactions of the American Society of Mechanical Engineers, Journal of Vibration and Acoustics* **109**, 144–151. Measurement of hydrodynamic interaction matrices of boiler feed pump impellers.
17. G. Jacquet-Richardet, G. Ferraris and P. Rieutord 1996 *Journal of Sound and Vibration* **191**, 901–915. Frequencies and modes of rotating flexible bladed-disc–shaft assemblies: a global cyclic symmetry approach.
18. G. Jacquet-Richardet, G. Ferraris and P. Rieutord 1995 *Transactions of the American Society of Mechanical Engineers, Technical Conference DE* **84-2**, 1215–1220. A numerical method for the dynamic analysis of rotating flexible blade–disc–shaft assemblies.
19. N. Maman and C. Farhat 1995 *Computers and Structures* **54**, 779–785. Matching fluid and structure meshes for aeroelastic computations: a parallel approach.
20. G. P. Guruswany 1989 *American Institute of Aeronautics and Astronautics Journal* **27**, 788–793. Integrated approach for active coupling of structure and fluids.
21. F. Moyroud, G. Jacquet-Richardet and T. H. Fransson 1996 *Transactions of the American Society of Mechanical Engineers, Paper*. 96-*GT*-335. A modal coupling for fluid and structure analysis of turbomachinery flutter: application to a fan stage.
22. Y. M. Xie 1996 *Journal of Sound and Vibration* **192**, 321–331. Assessment of time integration schemes for non linear dynamic equations.
23. O. Bonneau 1989 *Thèse de doctorat no*. 219, *Université de Poitiers*. Comportement statique et dynamique de ligne d'arbre montée sur palier fluide: influence des caractéristiques de palier.
24. P. Rieutord 1996 *Thèse de doctorat* 96 *ISAL* 7: *Institute National des Sciences Appliquées*. Comportement dynamique des rotors de turbomachines avec couplage fluide-structure: modélisation tridimensionnelle.

25. A. BERLIOZ, R. HENRY, J. M. PUGNET and G. FERRARIS 1990 *Proceedings of the 3rd International Conference on Rotordynamics IFToMM*, 10–12 *September*, *Lyon* 403–409; Editions du CNRS. Experimental and theoretical dynamic analysis of a rotating shrouded impeller.

APPENDIX: DECOMPOSITION OF A FULL NODAL FORCES VECTOR INTO CYCLIC SYMMETRICAL FORCES VECTORS

The nodal forces $\{F\}$ are given for the whole structure. In order to be consistent with a cyclic symmetrical formulation, vector $\{F\}$ can always be written for each sector p as

$$\{F^{(p)}\} = \sum_{n=0}^{N^*/2} (\{F_n^c\} \cos (p-1)\beta_n + \{F_n^s\} \sin (p-1)\beta_n), \tag{A1}$$

where N is the total number of cyclic sectors and $N^* = N$ if N is even or $N^* = N - 1$ if N is odd. Vectors $\{F_n^c\}$ and $\{F_n^s\}$ are obtained after a discrete Fourrier decomposition of $\{F\}$,

$$\{F_n^c\} = A_n \sum_{p=1}^{N} \{F^{(p)}\} \cos \frac{2\pi}{N} (p-1)n, \qquad \{F_n^s\} = A_n \sum_{p=1}^{N} \{F^{(p)}\} \sin \frac{2\pi}{N} (p-1)n, \tag{A2, A3}$$

with $A_n = 2/N$ if $n \neq 0$ or $n \neq N/2$, and $A_n = 1/N$ otherwise.

After decomposition, $N^*/2$ different dynamic problems are solved. Then the real displacement vector is obtained by recomposition of the different displacement terms of the series

$$\{\delta^{(p)}\} = \sum_{n=0}^{N^*/2} \{\delta_n^{(p)}\} = \sum_{n=0}^{N^*/2} (\{\delta_n^c\} \cos (p-1)\beta_n + \{\delta_n^s\} \sin (p-1)\beta_n). \tag{A4}$$